JGR Planets

RESEARCH ARTICLE
10.1029/2020JE006416

Key Points:

- Slepian orthonormal functions are used to estimate the localized short-scale gravity field of Jupiter using Juno observations
- The determination of Jupiter's gravity field is tailored to the geometry of the Juno orbit
- The measured localized short-scale gravity field of Jupiter matches the prediction from a thermal wind model of the zonal jets

Supporting Information:

- Supporting Information S1
- Data Set S1
- Data Set S2
- Data Set S3
- Data Set S4
- Data Set S5
- Data Set S6
- Data Set S7
- Data Set S8

Correspondence to:
M. Parisi,
marzia.parisi@jpl.nasa.gov

Citation:
Parisi, M., Galanti, E., Folkner, W. M., Kaspi, Y., & Buccino, D. R. (2020). Resolving the latitudinal short-scale gravity field of Jupiter using Slepian functions. *Journal of Geophysical Research: Planets*, *125*, e2020JE006416. https://doi.org/10.1029/2020JE006416

Received 24 FEB 2020
Accepted 24 SEP 2020

Resolving the Latitudinal Short-Scale Gravity Field of Jupiter Using Slepian Functions

Marzia Parisi[1], Eli Galanti[2], William M. Folkner[1], Yohai Kaspi[2], and Dustin R. Buccino[1]

[1]Jet Propulsion Laboratory, California Institute of Technology, Pasadena, CA, USA, [2]Department of Earth and Planetary Sciences, Weizmann Institute of Science, Rehovot, Israel

Abstract Early gravity measurements performed by the *Juno* spacecraft determined Jupiter's low-degree gravity harmonics, including the first estimate of the planet's north-south asymmetric field. The retrieved information was used to infer that the strong zonal winds visible at the cloud tops must extend down a few thousand kilometers, where they are suppressed in the deep interior. The next frontier for the Juno gravity experiment includes, among other goals, the determination of Jupiter's small-scale gravity field with high accuracy, and its relation to atmospheric circulation at shorter length scales. The geometry of the Juno closest approaches to the planet poses a challenge to this task, as they span latitudes between 4°N and 29°N over the course of the nominal mission. Since Doppler measurements are the most sensitive to gravity anomalies when the spacecraft is close to the body, observations of Jupiter's gravity field are mostly concentrated in the northern hemisphere, while the traditional spherical harmonic functions are not orthonormal over a latitudinal subdomain. Here we define customized Slepian functions, which are orthogonal in a specific latitude range and are optimized to represent Jupiter's local surface gravity at north latitudes. We show that with the new functions, the short-scale latitudinal variability of the gravity field is resolved with high accuracy between 15°S and 45°N latitude. Furthermore, preliminary results show that the estimated values for the Slepian coefficients from the Juno data match the predictions obtained using thermal wind balance to relate the dynamical density anomalies and the winds with an optimized scale height.

Plain Language Summary Among the main scientific objectives of NASA's Juno mission is the determination of Jupiter's gravity field with high accuracy. The measurements are related to the planet's internal mass distribution and carry information about its structure and dynamics below the visible clouds. Gravity science observations from the first few close flybys of the spacecraft allowed for the determination of the long-scale, global gravity field of the planet with unprecedented accuracy. On the other hand, the determination of the short-scale, localized gravity field is challenging when using the traditional spherical harmonic function basis used in planetary geodesy. In fact, these functions are defined globally, whereas the Juno observations are geographically limited to the northern hemisphere. In this work we use the Slepian function basis, which is defined over a limited latitudinal region of the planet, to resolve the small scale variability of the northern gravity field of Jupiter.

1. Introduction

The gravity field of Jupiter is a mosaic of different effects of diverse origin. It has contributions primarily from the fast uniform rotation of the deep interior, synchronous with Jupiter System III, and from the strong and deep zonal winds, characterized by east-west relative velocities with respect to the solid-body rotation (Kaspi et al., 2018). Deviations from the field of a homogeneous sphere due to the former are symmetric with respect to the equatorial plane of Jupiter, much like the centrifugal acceleration. The uniform rotation response of the planet decays rapidly as a function of the harmonic degree, with the zonal coefficient of degree 10 being four orders of magnitude smaller than the degree two coefficient (Hubbard, 1999). On the other hand, the profile of the spherical harmonic coefficients from zonal flows is more uniform, with a difference between degrees 2 and 25 of two orders of magnitude at most, depending on the winds' scale height (Kaspi et al., 2010). More importantly, the latitudinal profile of the Jovian winds is not north-south symmetric (Chapman, 1969), potentially giving rise to an odd gravity field if

sufficiently deep. Prior to the *Juno* measurements, it was postulated that atmospheric dynamics could lead to a detectable antisymmetric gravity field (Kaspi, 2013). One of the main scientific achievements of the Juno gravity experiment is the measurement of Jupiter's odd harmonics at low degrees, and relating their magnitude to the vertical extension of the winds within the planet's interior. The first two closest approaches of the Juno spacecraft, or perijoves, dedicated to gravity measurements (labeled as PJ3 and PJ6) were capable of answering this long standing question. The first nine zonal harmonics (J_2–J_{10}) were measured by Doppler tracking of the spacecraft (Iess et al., 2018) and the values of the odd coefficients were input to an adjoint optimization algorithm (Galanti & Kaspi, 2016) in order to determine the depth of the winds. The analysis yielded a wind depth of about 3,000 km below the visible cloud tops (Kaspi et al., 2018).

In addition to the odd gravity signal, the high-degree gravity field of Jupiter ($l > 10$) also contains valuable information about the planet's atmospheric dynamics. Beyond degree 10, the contributions to the gravity field from winds is dominant compared to uniform rotation and the coefficients are expected to be tied to the local, short-scale structure of the jets (Kaspi et al., 2010). The geometry of the Juno science orbits renders challenging the recovery of the spherical harmonic coefficients of degree higher than 10 with the necessary accuracy. The point of closest approach between the spacecraft and the planet occurs every 53 days at altitudes between 3,500 and 8,000 km over the cloud tops. Juno is sampling Jovian latitudes between 4°N and 29°N during the span of the nominal prime mission (first 33 orbits), with the perijove latitude shifting northwards by ~1° per orbit. Doppler measurements of the spacecraft velocity are strongly affected by the gravity field of Jupiter when close to the planet, therefore the data set available for gravity analysis is strongly skewed toward the northern hemisphere, specifically in a spherical belt comprised between latitudes 15°S and 45°N.

The spherical harmonic functions, used in the gravity analysis, are not orthogonal over the latitudinal domain over which the Juno measurements are mostly available. Estimates of high-degree spherical harmonic coefficients obtained from measurements made over a bounded domain suffer from undesirable coupling (Simons & Dahlen, 2006; Wieczorek & Simons, 2005), which leads to an increase in the formal uncertainties in the parameter estimation. In this paper, we explore the advantages of adopting a different function basis to represent the localized, high-degree gravity field of Jupiter, namely Slepian functions, that are orthonormal over a limited latitudinal band. The low-degree (2–10) spherical harmonics are still used to describe the large-scale gravity field, whose signal is large enough that Juno can measure it globally with good accuracy (Iess et al., 2018). Slepian functions are defined as linear combinations of spherical harmonics and we select the ones which take significant values only within the chosen bounded domain, while being very small outside of it (Albertella et al., 1999; Simons et al., 2009). This method was already proved useful for mapping the mass loss of Greenland by (Harig & Simons, 2012), where the choice of a limited domain for the observations is dictated by the discrete nature of the mass anomaly rather than by the orbit geometry. Using a similar approach, Galanti et al. (2019) study the potential of detecting the local gravity signature of Jupiter's Great Red Spot using dedicated Juno orbits. Analogously to what was done by Kaspi et al. (2010) and Kaspi (2013) for spherical harmonics, we can expand the gravity perturbations from winds for a given scale height, using the Slepian basis. We can then assess the detectability of their signal by the Juno gravity experiment. Measurements of the higher frequency gravity field from atmospheric dynamics will complement the measurements of the global depth of the winds from low-degree odd harmonics by Kaspi et al. (2018) and potentially add information about the short-scale structure of the zonal winds.

The paper is organized as follows. In Section 2, we discuss the current Juno gravity solution halfway through its nominal mission, using the traditional spherical harmonic approach, and explain why the recovery of the high-degree coefficients is challenging. In Section 3, we introduce the Slepian functions as linear combinations of the spherical harmonic functions optimized for the Juno gravity science case. In Section 4 we discuss the expected gravity signal from the winds in terms of the Slepian functions, in order to predict the expected values for the coefficients as a function of the wind depth. In Section 5 we compare these predictions to the actual Juno measurements of the Slepian coefficients and in Section 6 we present our conclusions and discussion.

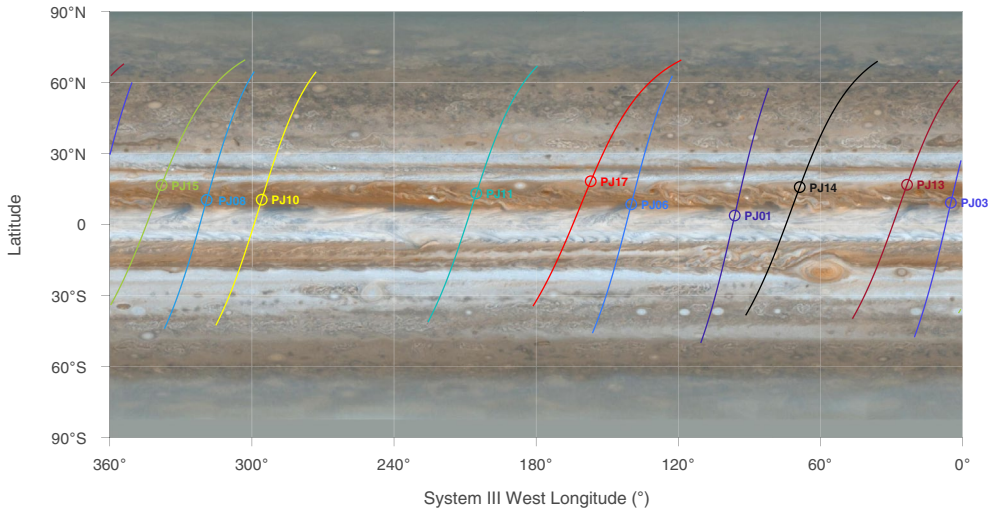

Figure 1. Juno's 10 gravity science ground tracks among the first 17 perijoves, displayed on a Jovian map of the visible clouds as a function of latitude and west longitude. The closest approach latitudes (unfilled circles) are contained within a limited belt in the northern hemisphere. The background image is based on Cassini narrow-angle camera observations of Jupiter's visible clouds during the flyby in December 2000. Background image credit: NASA/JPL/Space Science Institute.

2. The Spherical Harmonic Coefficients of Jupiter's Gravity Field

In this section we present the traditional spherical harmonic approach to the estimation of Jupiter's gravity field. Our analysis combines Juno data from the first 17 science orbits, 10 of which were devoted to gravity measurements and occurred between August 2016 and December 2018. Similarly to what was done by Folkner et al. (2017), Iess et al. (2018) and, most recently, Durante et al. (2020), we start by describing the estimation process employed to retrieve the gravity coefficients characterizing the gas giant. The Juno orbit around Jupiter is very eccentric (0.98) and the spacecraft encounters the planet at close range every 53 days for a time window of a few hours. During the closest approaches, the Gravity Science instrument (Asmar et al., 2017) is extremely sensitive to perturbations in the spacecraft's radial velocity, which are related to the subtle variations in the gravity field of Jupiter.

The main observable for the Juno gravity experiment is the two-way Doppler shift on the radio carriers, enabled by the on-board radio system, which features dual-frequency links with the ground stations of NASA's Deep Space Network. In our analysis we used X- and Ka-band data (7.2–8.4 GHz and 32.5–34 GHz, respectively), received and transmitted through the on-board high-gain antenna. Our data set encompasses measurements collected during science orbits labeled as perijoves number 1, 3, 6, 8, 10, 11, 13, 14, 15, and 17. Most of the data were collected with the 34-m DSS 25 and DSS 26 antennas in Goldstone, except for PJ1, which was visible from the Madrid complex (Folkner et al., 2017). Of these 10 gravity passes, eight utilized the dual-frequency uplink and dual-frequency downlink configuration, while PJ1 and PJ13 utilized single-frequency uplink at X-band and dual-frequency downlink. In the time frame of these perijoves, the closest approaches occurred at latitudes between 4°N and 18°N at various Jovian longitudes (Figure 1) and altitudes as low as 3,500 km over the planet's upper atmosphere (Durante et al., 2020).

The dual-frequency link on both communication legs allows for the cancellation of up to 75% of plasma noise (50% if the uplink is single-frequency), due, among other effects, to the crossing of the Io Plasma Torus by the radio signals around perijoves (Phipps et al., 2019). Other sources of noise are from the Earth's troposphere and ionosphere. The former can be partially calibrated using empirical models of the atmosphere or measurements of the water vapor content with radiometers located at Goldstone (Asmar et al., 2005). The latter is modeled on the basis of Global Positioning System (GPS) observations. The root mean square of the one-way line-of-sight velocity residuals varies from a minimum of about 5 $\mu m\ s^{-1}$ for PJ11 to a maximum of 53 $\mu m\ s^{-1}$ for PJ1, at 60 s integration time, while most perijoves fall within the range 5–10 $\mu m\ s^{-1}$.

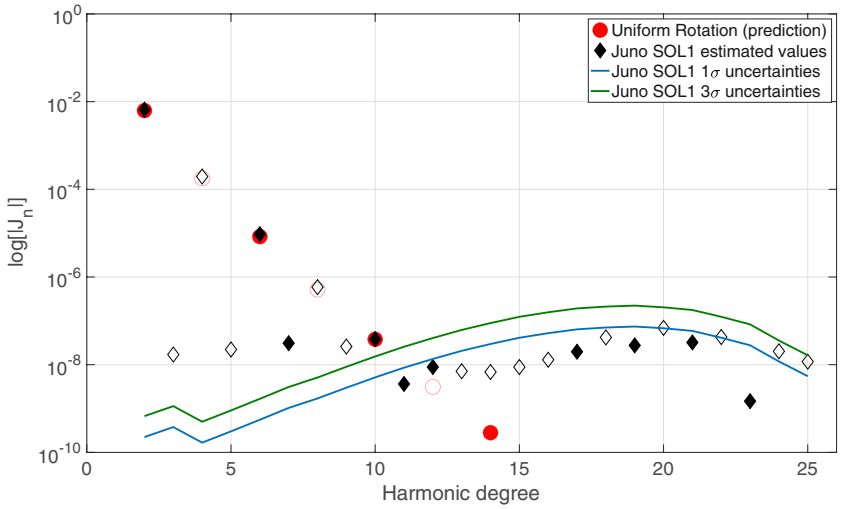

Figure 2. Spherical harmonic coefficients of Jupiter's gravity field estimated from Juno data collected during the first 17 perijoves (SOL1), as a function of the harmonic degree. The y-axis shows the normalized coefficients on a logarithmic scale. The black diamonds indicate the estimates for J_2–J_{25}. Red circles represent the predicted contributions to the gravity field with an equipotential model at rigid-body rotation (Hubbard, 1999). The markers are filled (positive) or unfilled (negative) depending on the sign. The blue and green solid lines represent the 1σ and 3σ formal uncertainties from Juno measurements, respectively.

The dynamical model used to integrate the Juno trajectory for orbit determination purposes accounts for several effects due to gravitational and nongravitational forces acting on the spacecraft. A nonexhaustive list is: the mass of Jupiter, the Sun and the other planets (Folkner, 2019); Jupiter's rotational parameters (Archinal et al., 2010); Jupiter's zonal harmonic coefficients from degree 2 to 12 (Iess et al., 2018); tidal perturbations caused by the Galilean satellites up to degree 6 (Wahl et al., 2020); the mass of the Galilean satellites (Jacobson, 2013); solar pressure radiation; Jupiter's albedo and thermal emission from the planet.

Doppler data at 60 s integration time from the 10 gravity perijoves are combined in a multiarc square-root information filter, in order to obtain a least-square estimate and covariance of the physical parameters that characterize Jupiter's gravity. This approach is equivalent to what was presented by Iess et al. (2018) and Durante et al. (2020). Figure 2 shows the normalized estimated values, and the corresponding 1σ and 3σ uncertainties, for the first 25 spherical harmonic coefficients which describe the axially symmetric gravity field of the planet. We label this solution as SOL1. The values are consistent with the one reported by Iess et al. (2018) and Durante et al. (2020), except for a slight difference in the value of J_2, due to different considerations used to account for the permanent tide raised by the Galilean satellites, not relevant to this study. The estimates for J_2–J_{10} (black diamonds) are well above the 1σ and 3σ levels (blue and green solid lines, respectively). As expected, the contribution to the even-degree harmonics from uniform rotation decays rapidly with the harmonic degree (Hubbard, 1999), while the values of the odd harmonics, which were used by Kaspi et al. (2018) to infer the vertical extension of the winds, do not decay at higher frequencies. Beyond degree 11, the estimated values for SOL1 lie all below the 3σ level, in some cases by as much as one order of magnitude.

A different way of looking at the recovery of Jupiter's gravity is plotting the measured surface gravity and its uncertainty as a function of latitude. Figure 3 shows the residual gravity calculated using the coefficients J_3, J_5, J_7, J_9–J_{25} and their covariance as estimated in SOL1. We omit the contribution from J_2, J_4, J_6, J_8 to the surface gravity in order to remove the biggest effects from uniform rotation (contributions from the winds to these four coefficients are negligible in comparison). In calculating the formal uncertainty in Jupiter's surface gravity, we account for the coupling among all estimated spherical harmonic coefficients, which affect both the central value and the uncertainty bounds. Within the latitudinal band 5°N–20°N, the uncertainties

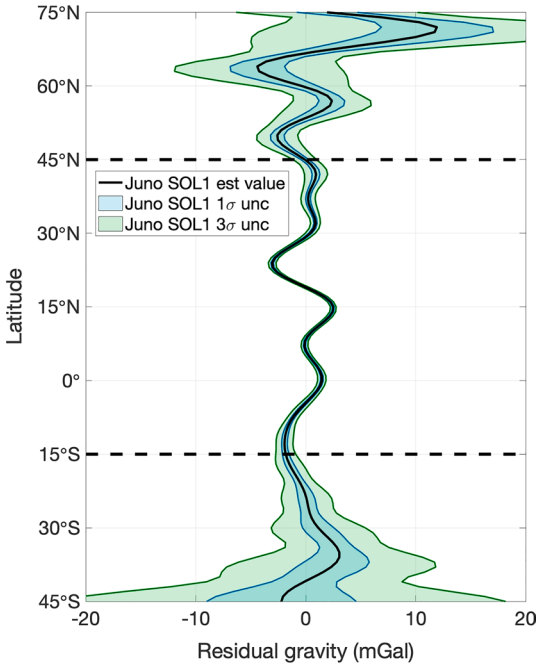

Figure 3. Jupiter's asymmetric and high-degree surface gravity from J_3, J_5, J_7, J_9–J_{25}, as a function of latitude and defined with respect to the homogeneous sphere (shown for the range 45°S–75°N), from PJ1-PJ17 Juno gravity data analysis (SOL1). The light blue and green shaded areas represent the 1σ and 3σ uncertainties, respectively. The horizontal dashed lines show the region where the surface gravity is known with high accuracy (<1 mGal).

on the gravity disturbances are as low as 0.1 mGal (Durante et al., 2020), whereas they reach values of several mGals between 45°S–5°N and 20°N–75°N. The surface gravity in the polar regions is not shown in Figure 3, since the uncertainties reach values as high as hundreds of mGal, due to the geometry of the Juno orbit. The gravity field of Jupiter between latitudes 15°S and 45°N is very well determined, due to the proximity of the spacecraft to the planet during closest approach. As the spacecraft continues to collect observations of the gravity field, we are bound to obtain more precise observations of the northern hemisphere, whereas observations in the southern hemisphere are still precluded.

In summary, while the low-degree gravity field is accurately determined by Juno, it is challenging to estimate the high-degree, small-scale gravity field of Jupiter (J_{11}–J_{25}) using the traditional approach with spherical harmonic functions (SOL1). The reason is the limited range of latitudes in which the Juno perijoves occurred (4°N–18°N), where the spacecraft trajectory is sensitive to subtle perturbations in the gravity field of Jupiter. In a bounded latitude range, spherical harmonics are not orthogonal and the large correlations between the high-degree coefficients result in high correlated uncertainties. The Juno gravity data does contain information about the short-scale perturbations of the gravity field of Jupiter in the northern hemisphere, however the estimation using zonal harmonics only results in much of the information being represented by correlation coefficients rather than the estimated central values. The decrease in the uncertainty values after J_{20} is an artifact of the truncation of the spherical harmonic estimation at degree 25. Since the higher degree estimates are not available, they cannot be factored into the calculation of the coupling among parameters. For harmonic degrees beyond 10, the gravity signal from the winds is expected to dominate in comparison to the contribution from uniform rotation (Hubbard, 1999; Kaspi, 2013; Kaspi et al., 2010). The detection of such parameters would allow for the study of the shorter-scale dynamics and to assess whether their behavior is similar to the large-scale dynamics, as extrapolated from the analysis of the odd harmonics (Kaspi et al., 2018; 2020).

3. Slepian Functions over a Bounded Latitudinal Domain

The results shown in Section 2 suggest that a different function basis, which is orthonormal in a band-limited domain, may be used to better exploit the localized information on Jupiter's gravity from the Juno observations. Such are the Slepian functions, which have largely been used in space and Earth geodesy when the observations are not uniformly spread over the latitudinal domain (Simons & Dahlen, 2006) or when the mass anomaly is localized (Harig & Simons, 2012).

In this paper we follow the derivation from Albertella et al. (1999), which defined the problem of orthonormality over a spherical belt in the domain $B = \{0 \le \lambda < 2\pi, \theta_1 \le \theta \le \theta_2\}$, where λ is the longitude and θ is the latitude. The optimization problem consists of maximizing the information carried by a function T over the domain B, or, analogously, minimizing the cost function (Albertella et al., 1999):

$$J(T) = \frac{\frac{1}{4\pi}\int_B T^2 d\sigma}{\frac{1}{4\pi}\int_\sigma T^2 d\sigma} = \frac{\sum_{n,m,j,k} T_{nm} K^B_{nmjk} T_{jk}}{\sum_{n,m} T^2_{nm}}, \quad (1)$$

where $d\sigma$ is the element of the surface σ of unit radius, and K^B_{nmjk} is the Gram-Schmidt matrix of the original set of functions. In our case these are spherical harmonics $\{Y_{nm}, |m| \le n \le N\}$, therefore:

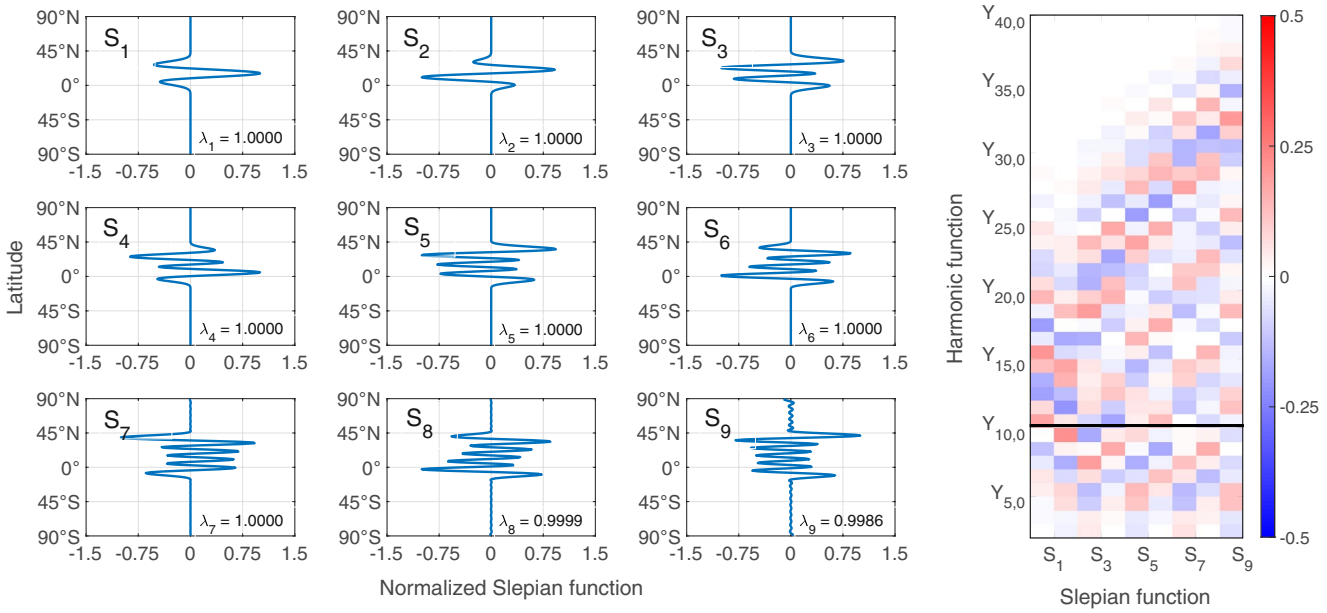

Figure 4. Left panels: the nine Slepian functions defined by the transformation in Equation (4), and which are concentrated in the latitudinal band 15°S < θ < 45°N. They are generated by combining zonal spherical harmonics from degree 2 to 40. We named the functions S_1–S_9 and indicated the corresponding eigenvalue in each plot. Right panel: correlation matrix between the nine significant Slepian functions S_1–S_9 (x-axis) and zonal harmonic functions $Y_{2,0}$–$Y_{40,0}$ (y-axis), over latitudes 90°S–90°N. All the coefficients have maximum absolute values below 0.25.

$$K^B_{nmjk} = \frac{1}{4\pi}\int_B Y_{nm}(\sigma)Y_{jk}(\sigma)d\sigma. \tag{2}$$

The matrix defined in Equation (2) can be diagonalized, by finding its eigenvectors $\boldsymbol{a}^m_n$ and corresponding eigenvalues α^m_n. The matrix of eigenvectors A^m (whose columns are eigenvectors) is used to rotate the original basis functions Y_{nm} into the new basis functions S_{jm} (Albertella et al., 1999):

$$S_{jm}(\sigma) = \sum_{n=|m|}^{N} a^{m+}_n Y_{nm}(\sigma) \quad \{\text{for } j = |m|,\ldots,N\}, \tag{3}$$

where S_{jm} are the Slepian functions of degree j and order m. The word degree, when referred to Slepian functions, does not have the same meaning as for homogeneous polynomials, and is assigned by analogy only (Albertella et al., 1999). Every Slepian function of degree j is the linear combination of spherical harmonics of the same order m, up to a maximum degree N, which is set to 40 in this work. This formulation is capable of maximizing the information over the selected latitudinal belt. As such, Slepian functions are not associated with a single wavelength, or physical length scale in the sense of periodic functions, as for spherical harmonics (Albertella et al., 1999).

For our application to the Juno measurements of Jupiter's gravitational potential, we set 15°S < θ < 45°N, which is the latitudinal region where the surface gravity is known with accuracies (1σ) better than 1 mGal (Figure 3). We define N as the maximum spherical harmonic degree used to generate the Slepian functions (Albertella et al., 1999). We chose $N = 40$ and $m = 0$ to build the matrix K in Equation 2. This means that each Slepian function, obtained by varying the index j in the left hand side of Equation 4, is a linear combination of zonal spherical harmonics only, from $Y_{2,0}$ to $Y_{40,0}$. Note that in this case the functions $Y_{n,0}$ are the zonal harmonics of degree n. Only Slepian functions associated with eigenvalues larger than 0.99 are considered localized in the latitude range and are selected for our analysis. The left panels in Figure 4 show the 9 (out of 39) normalized Slepian functions which are significant in the selected latitudinal belt and are very small elsewhere (as little as 1% of the functions' spectral energy is spread outside of the chosen domain), as a function of latitude. Traditionally, Slepian functions are ordered by decreasing

eigenvalue and labeled using their rank, with one being associated with the more concentrated function and so forth. We name the functions S_1–S_9, characterized by decreasing spatial scales (and eigenvalues) or increasing number of zero crossings within the limited latitudinal domain. The structure of function S_1 is comparable to the zonal harmonic function $Y_{10,0}$, after the latter has been multiplied by a window function which is zero outside of the same latitudinal band. However, the number of zero-crossings between latitudes 15°S and 45°N of the Slepian functions increases faster than for spherical harmonics in the same region.

The right panel in Figure 4 shows the power of the expansion coefficients of the Slepian functions (S_1–S_9) in the spherical harmonic basis used to define them (Y_2–Y_{40}). These parameters were calculated by multiplying each spherical harmonic function with each Slepian function and evaluating the integral of the product. All the coefficients have values that are smaller than 0.25, indicating negligible overlap between the spherical harmonics and the Slepian functions, over the whole latitudinal domain 90°S–90°N (see Supporting Information S1). Of particular interest are the small correlations between the low-degree spherical harmonic functions $Y_{2,0}$–$Y_{10,0}$ and S_1–S_9 indicated on Figure 4, for reasons that will be explained in Section 5. In reality, when reducing Juno data in the least-square filter, the correlation coefficients among the estimated parameters and derived from the information matrix will have different values than the expansion coefficients in Figure 4, as they take into account several additional effects, such as the data noise level and the geometry of the orbit.

A direct way to estimate the number of Slepian functions that are sufficiently concentrated in the domain of interest is to calculate the Shannon number, which is a function of the ratio between the fractional area A of the spherical segment defined by the latitudinal band and the area of the whole sphere (Simons et al., 2006). The Shannon number is also equivalent to the sum of the eigenvalues (λ_i) of the matrix K and is calculated as follows (Galanti et al., 2019; Simons et al., 2006):

$$\sum_{i=1}^{(L+1)^2} \lambda_i = (L+1)^2 \frac{A}{4\pi} \tag{4}$$

where $(L+1)^2$ is the number of spherical harmonic functions used to defined the Slepian functions in the limited domain. The Shannon number for the case considered in Figure 4 is approximately 13, although only the nine highest ranking Slepian functions satisfy our requirement that 99% of the function power be concentrated in the limited latitudinal belt (eigenvalues > 0.99).

4. Projection of the Short-Scale Gravitational Signal from the Winds onto the Slepian Basis

Following Kaspi et al. (2018), we calculate the density perturbations ρ' due to atmospheric dynamics visible in Figure 1, using the thermal wind equation:

$$2\boldsymbol{\Omega} \cdot \nabla(\tilde{\rho} v) = \nabla \rho' \times \boldsymbol{g}, \tag{5}$$

where $\boldsymbol{\Omega}$ is the planet's rigid-body angular velocity, $\tilde{\rho}$ is the hydrostatic density, $\boldsymbol{v}$ is the wind velocity and $\boldsymbol{g}$ is the gravitational acceleration. The equation holds because the Rossby number for Jupiter is small, meaning the Coriolis acceleration is balanced, to leading order, by the horizontal pressure gradient. For this calculation, we define the flow field as:

$$u(r,\theta) = u_{\mathrm{cyl}}(r,\theta) e^{-\frac{R_J - r}{H}}, \tag{6}$$

where u is the east-west (longitudinal) velocity component, r is the radial direction and θ is the latitude. u_{cyl} is the velocity profile obtained by extending the observed cloud level wind (Tollefson et al., 2017) along the direction of the rotation axis (Kaspi et al., 2009), and R_J is Jupiter's equatorial 1-bar radius. The wind decays exponentially in the radial direction according to the scale height H. Note that the optimal solution for the

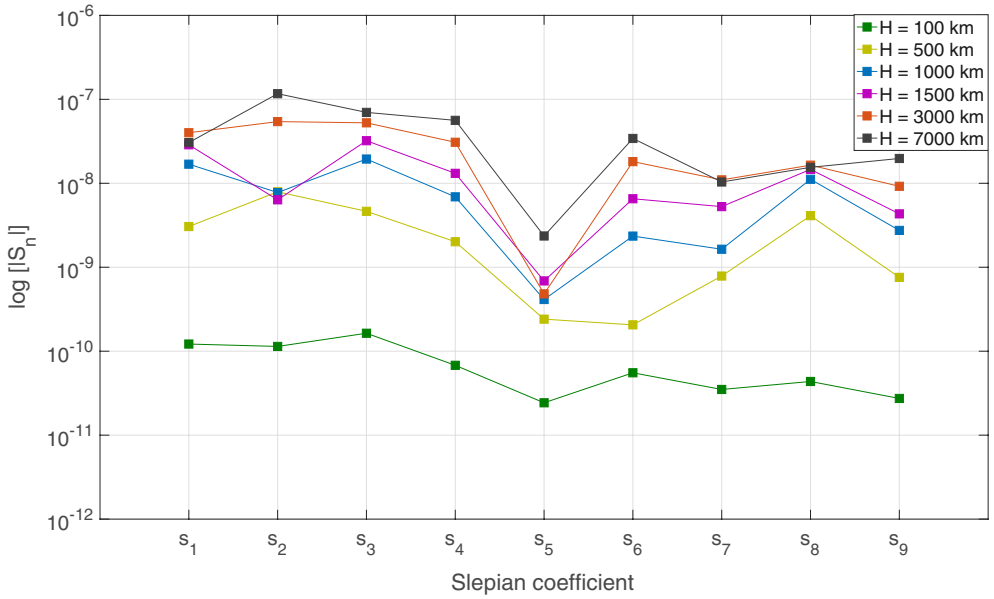

Figure 5. Predicted values for the Slepian coefficients s_1–s_9 using the thermal wind method, for scale heights between 100 and 7,000 km. The signs of the coefficients are ignored in this plot, with the main focus being the amplitude of the wind signal. The y-axis shows the logarithm of the absolute value of the normalized coefficients.

low-order gravity harmonics was found using more complex vertical decay functions than the exponential decay used here (Kaspi et al., 2020). However, for the purpose of this study the e-folding function gives a reasonable representation of the deep dynamics of the winds.

Solving Equation 5 for ρ′ (Parisi et al., 2016; 2020), the wind-induced contributions to the gravitational potential due to atmospheric perturbations are obtained in terms of spherical harmonics (Kaspi et al., 2010):

$$\Delta J_n = \frac{1}{MR_J^n}\int_0^{R_J} r^{2+n}dr \int_0^{2\pi} d\phi \int_{-1}^{1} P_j(\mu)\rho' d\mu \quad \{\text{for } n = 0,\ldots,N\}, \tag{7}$$

where M is the planetary mass, r is the radial coordinate, μ is the cosine of the latitude and N is the maximum degree considered (in this work $N = 40$). These contributions can be projected onto the Slepian basis to determine the coefficients s_j of degree j related to the Slepian functions S_j. This is achieved by plugging Equation 7 into Equation 4:

$$s_j = \sum_{n=0}^{N} a_n^0 \frac{1}{MR_J^n}\int_0^{R_J} r^{2+n}dr \int_0^{2\pi} d\phi \int_{-1}^{1} Y_n(\mu)\rho' d\mu \quad \{\text{for } j = 0,\ldots,N\}, \tag{8}$$

where a_n^0 is the component of order-0 (zonal) of the n^{th} eigenvector of K (Equation 2).

In Figure 5 we calculate the contributions from the winds to the short-scale gravity field of Jupiter in the northern hemisphere, depending on their penetration depth, from a minimum H of 100 km to a maximum of 7,000 km. The deeper the winds (increasing H), the more the mass involved in the flow and the larger the magnitude of the Slepian coefficients, similar to the behavior of spherical harmonic coefficients shown by Kaspi (2013).

5. Juno Observations of Jupiter's Northern Gravity Field

Next, we examine the predictions for the Slepian coefficients assuming the winds are characterized by an e-folding scale height H of 1,500 km. This value is close to the best fit of the measured odd harmonics (J_3, J_5, J_7, J_9) from Juno gravity data assuming that the winds decay exponentially (Kaspi et al., 2020). Note that this

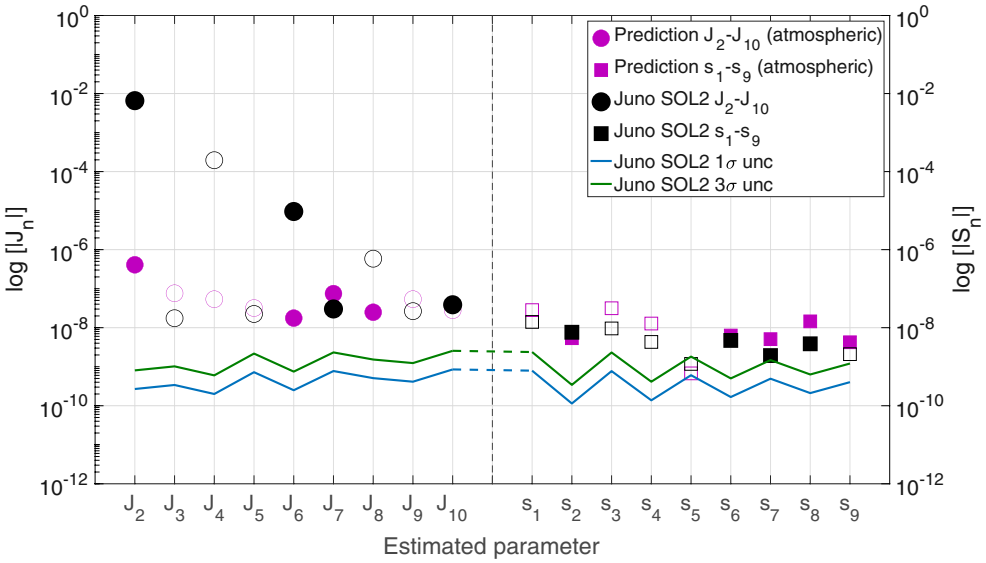

Figure 6. Solution for Jupiter's gravity field from Juno data (PJ1-PJ17), estimating a combination of low-degree spherical harmonics and Slepian functions (SOL2). The purple circles and squares indicate the coefficients from the thermal wind model with an exponential decay of the winds with depth, for a scale height of 1,500 km. The estimated values from Juno observations are represented by the black circles (normalized spherical harmonics) and squares (Slepian functions). Filled markers indicate positive values, while unfilled markers indicate negative values. The solid blue and green lines represent the 1σ and 3σ uncertainty levels, respectively. The measured values for s_1–s_9 match the predictions from thermal wind balance within the 3σ level.

is not the optimal profile capable of matching the observations and is used here for simplicity. In fact, the best matching profile is a more complex function which reaches down to about 3,000 km. However, for an exponential function (as in this study), the best matching value for H is around 1,500 km, considering that the winds extend deeper down for at least two scale heights.

We compare these predictions to the actual estimates for the Slepian coefficients, obtained by combining Juno Doppler data from PJ1-PJ17. In order to account for the new basis (Figure 4, left panels), we consider an augmented estimation case, labeled SOL2. The definition of the dynamical model is similar to SOL1 and the main difference is in the vector of solved-for parameters. Instead of estimating spherical harmonic coefficients J_2–J_{25}, we estimate a combination of low-degree spherical harmonics J_2–J_{10} and the Slepian coefficients s_1–s_9. Note that the theoretical correlations between the basis functions are below 0.25 (Figure 4, right panel), as such, although harmonic and Slepian functions are not strictly orthogonal to each other, the corresponding parameters can be estimated without concern for significant couplings between the two bases. Furthermore, the fact that our chosen set of Slepian functions are not orthogonal to low-degree spherical harmonics does not significantly detract from our goal of comparing estimated gravity field to atmospheric models. Because the Juno data set is concentrated in the northern hemisphere, even using functions that are mathematically orthogonal over the full latitude range, would lead to estimated amplitudes which are heavily correlated for higher degrees.

The estimated values for the combination of low-degree spherical harmonic and Slepian coefficients using Juno data from PJ1–PJ17 (SOL2) are shown in Figure 6. The solution for the spherical harmonic coefficients J_2–J_{10} (left side) is consistent with the corresponding parameters in SOL1 (Figure 2), except that the formal uncertainties for J_5–J_{10} are now smaller, which is likely due to the reduced number of solved-for parameters. As for the Slepian coefficients (right side), the magnitude of the estimated values matches that of the predictions, as well as their signs (filled markers represent positive coefficients, while unfilled markers are negative). Only s_9 has an opposite estimated sign to the prediction. Note that the corresponding Slepian function S_9 is, among the chosen set, the one characterized by the most energy (although still less than 1%) outside of the selected latitudinal band, which might explain the discrepancy (Figure 4). In addition, the central value for s_9 is less than four times its formal uncertainty. The remaining estimated values for the short-scale gravity field are all above the 3σ level (green line), sometimes by as much as one order of magnitude, with the exception of s_5, whose estimated value is very small and undetected. On the other hand,

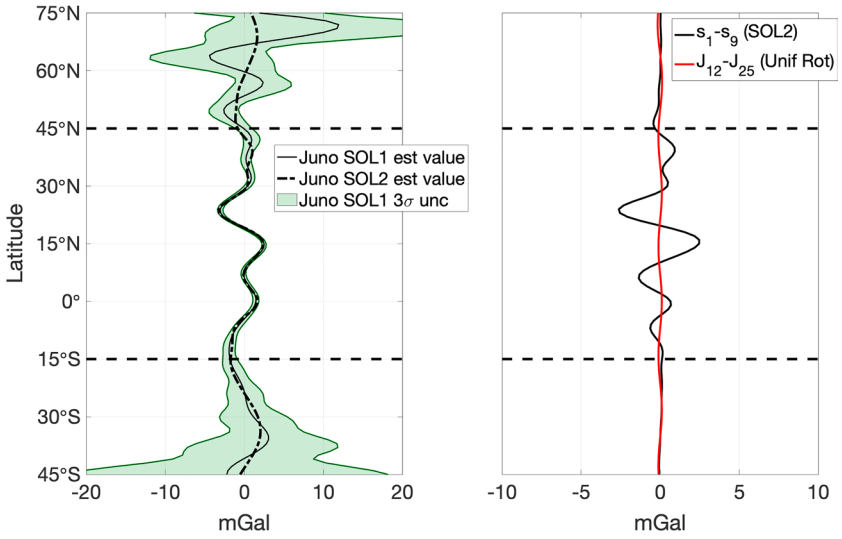

Figure 7. Left: surface gravity from the estimated spherical harmonic coefficients $J_{3,5,7,9-25}$ (black solid line, SOL1) and from the estimated low-degree spherical harmonics $J_{3,5,7,9}$ plus Slepian coefficients s_1–s_9 (black dash-point line, SOL2). The green shaded area represents the 3σ uncertainties on the estimated surface gravity (SOL 1). Right: the estimated short-scale surface gravity from Slepian coefficients s_1–s_9 only (black solid line, SOL2) and the predicted signal from uniform rotation from harmonics J_{12}–J_{25} (red solid line).

the predicted value for s_5 is small compared to the other coefficients regardless of the wind scale height, as shown by Figure 5. The correlations between estimated parameters belonging to different bases are included in the computation of the correlated covariance through the least-square reduction of the available data (Section S3 of the SI).

The comparison between Figures 2 and 6 highlights the advantage of using the Slepian basis, as it renders feasible the detection of the high-degree gravity field of Jupiter in the northern hemisphere. Furthermore, to first order, the short-scale circulation seems to be characterized by a depth of the same order as the large-scale flows. With that, the predicted values are mostly larger than the estimated values, indicating perhaps a shallower depth for the short-scale flows.

The left panel in Figure 7 shows Jupiter's residual gravity as calculated using the estimated spherical harmonics $J_{3,5,7,9-25}$ (black line, SOL1), its 3σ uncertainty (green shaded area, SOL1), and the surface gravity calculated from the estimated Slepian coefficients (s_1–s_9) plus low-degree spherical harmonic coefficients ($J_{3,5,7,9,10}$), represented by the dash-point black line (SOL2). The differences between the SOL1 and SOL2 surface gravity profiles are well below the 3σ level for latitudes between 15°S and 45°N, suggesting that the set of chosen Slepian functions is appropriate to describe Jupiter's gravity within the latitudinal range. Toward the poles, the profiles tend to diverge because of the different behavior of harmonic and Slepian functions outside of the spherical belt, although in this region the surface gravity is characterized by larger uncertainties as well.

Next, we compare the contributions to the surface gravity from s_1–s_9 alone (SOL2), to the predicted short-scale contributions from uniform rotation, which decay rapidly with the harmonic degree (Figure 7, right panel). Beyond degree 10, the contributions to the gravity field from uniform rotation (red solid line) are too small to explain the detected signal within the latitudinal band where the Juno observations are concentrated. Therefore, the measured high-degree gravity field is necessarily related to mass perturbations due to atmospheric dynamics.

6. Conclusion and Discussion

In this study we show that it is possible to detect the signature of Jupiter's short-scale zonal winds in the high-degree northern gravity field of the planet using Juno gravity measurements. Slepian functions are used for short-scale localized perturbations, while spherical harmonic functions are still used throughout

the analysis to estimate the low-degree, global gravity field of Jupiter. The new set of functions are orthonormal and the estimated values of their magnitude is well above zero in the spherical belt defined by latitudes 15°S < θ < 45°N, a subregion where the Juno orbit is closest to the planet's cloud level.

By combining the Juno gravity data from PJ1 to PJ17 we estimate nine Slepian coefficients describing the short-scale gravity field of Juno, most of which are resolved to better than the 3σ uncertainty level (except for s_5). The estimated values are compared to the predicted gravity signal from winds with $H = 1{,}500$ km, expanded in terms of Slepian functions. We find a remarkable match between the predictions and the observations, both in the central value and in sign (except for s_9). The accuracy associated with the Juno gravity measurements for latitudes between 15°S and 45°N is such that, as the winds are deeper than a few thousand kilometers, we are able to successfully detect the signature of atmospheric dynamics in the short-scale northern gravity field of Jupiter.

The underlying assumption is that the Juno sensitivity to short-scale gravity (degree-10 and beyond) is negligible outside the selected latitude band. In order to substantiate this assumption we consider the strength of the gravity signal, which decreases with the degree n like r^{n+2}, where r is the distance from the center of the planet. Since the orbit of Juno is very eccentric, the spacecraft flies over the poles (especially the south pole) at distances larger than 1.1 Jupiter radii, where the effect of J_{11} is at least 2.5 times weaker than at perijove. The comparison between the surface gravity profiles from SOL1 and SOL2 shown in Figure 7 (left panel), demonstrate that this assumption is valid within the accuracy level of the Juno gravity measurements.

A potential limitation of the method pertains the loss of orthogonality of Slepian functions far from the reference surface. The issue has been addressed by Galanti et al. (2019) for the study of the Great Red Spot with two Juno perijoves, where the authors concluded that for spacecraft altitudes below 0.2 Jupiter's radii (condition satisfied when Juno flies over Jovian latitudes comprised in 15°S < θ < 45°N), the degradation of the orthogonality of Slepian functions is negligible. This concern has also been addressed by Plattner and Simons (2017), who built optimal sets of spatiospectrally localized Slepian functions for observations carried out at variable altitude, such as Juno gravity measurements. They developed a method to balance out the noise increase due to downward continuation from the spacecraft location to the planetary surface. Another potential limitation comes from the correlations between the different gravity coefficients involved in the estimation process. Our analysis shows that the correlations between the high-degree zonal spherical harmonics ($Y_{n,0}$, n>10) are overall higher (>0.9 for some coefficients) than the correlations between the low-degree zonals ($Y_{n,0}$, $n \leq 10$) and the Slepian functions (S_j, $j = 1, ..., 9$) defined in this study (Figure 4, right panel). As a result, lower correlations imply smaller uncertainties in the estimation of the gravity coefficients.

Data Availability Statement

The Juno gravity data are publicly available through NASA's Planetary Data System at https://atmos.nmsu.edu/PDS/data/jnogrv_1001/ (Buccino et al., 2016). The geometrical data pertaining the Juno orbit is publicly available at https://naif.jpl.nasa.gov/naif/. All derived data produced in this research are available at: https://doi.org/10.5281/zenodo.3924390 (Parisi, 2020).

Acknowledgments
We thank the Juno Interior and Atmospheric Working Groups for the useful discussions. The research described in this paper was carried out at the Jet Propulsion Laboratory, California Institute of Technology, under a contract with the National Aeronautics and Space Administration (MP, WMF, and DRB) and at the Weizmann Institute of Science in Israel (EG and YK). EG and YK acknowledge support from the Israeli Space Agency, the Helen Kimel Center for Planetary Science and the Weizmann Institute of Science.

References

Albertella, A., Sansò, F., & Sneeuw, N. (1999). Band-limited functions on a bounded spherical domain: The slepian problem on the sphere. *Journal of Geodesy*, *73*(9), 436–447. https://doi.org/10.1007/PL00003999

Archinal, B. A., A'Hearn, M. F., Bowell, E., Conrad, A., Consolmagno, G. J., Courtin, R., et al. (2010). Report of the IAU working group on cartographic coordinates and rotational elements: 2009. *Celestial Mechanics and Dynamical Astronomy*, *109*, 101–135. https://doi.org/10.1007/s10569-010-9320-4

Asmar, S. W., Armstrong, J. W., Iess, L., & Tortora, P. (2005). Spacecraft Doppler tracking: Noise budget and accuracy achievable in precision radio science observations. *Radio Science*, *40*(2). https://doi.org/10.1029/2004RS003101

Asmar, S. W., Bolton, S. J., Buccino, D. R., Cornish, T. P., Folkner, W. M., Formaro, R., et al. (2017). The Juno gravity science instrument. *Space Science Reviews*, *213*, 205–218. https://doi.org/10.1007/s11214-017-0428-7

Buccino, D. R. (2016). Juno jupiter gravity science raw data set V1.0, JUNO-J-RSS-1 JUGR-V1.0, NASA planetary data system (PDS). Retrieved from https://atmos.nmsu.edu/PDS/data/jnogrv_1001/

Chapman, C. R. (1969). Jupiter's zonal winds: Variations with latitude. *Journal of the Atmospheric Sciences*, *26*, 986–990. https://doi.org/10.1175/1520-0469(1969)026<0986:JZWVWL>2.0.CO;2

Durante, D., Parisi, M., Serra, D., Zannoni, M., Notaro, V., & Racioppa, P. (2020). Jupiter's gravity field halfway through the Juno mission. *Geophysical Research Letters*, *47*(4), e2019GL086572. https://doi.org/10.1029/2019GL086572

Folkner, W. M. (2019). DE438 planetary ephemeris release notes. Retrieved from https://naif.jpl.nasa.gov/pub/naif/JUNO/kernels/spk/de438s.bsp.lbl

Folkner, W. M., Iess, L., Anderson, J. D., Asmar, S. W., Buccino, D. R., Durante, D., et al. (2017). Jupiter gravity field estimated from the first two Juno orbits. *Geophysical Research Letters*, *44*(10), 4694–4700. https://doi.org/10.1002/2017GL073140

Galanti, E., & Kaspi, Y. (2016). An adjoint-based method for the inversion of the Juno and Cassini gravity measurements into wind fields. *The Astrophysical Journal*, *820*(2), 91–100. https://doi.org/10.3847/0004-637X/820/2/91

Galanti, E., Kaspi, Y., Simons, F. J., Durante, D., Parisi, M., & Bolton, S. J. (2019). Determining the depth of Jupiter's Great Red Spot with Juno: A slepian approach. *The Astronomical Journal Letters*, *874*(2). https://doi.org/10.3847/2041-8213/ab1086

Harig, C., & Simons, F. J. (2012). Mapping Greenland's mass loss in space and time. *Proceedings of the National Academy of Sciences*, *109*(49), 19934–19937. https://doi.org/10.1073/pnas.1206785109

Hubbard, W. B. (1999). Gravitational signature of Jupiter's deep zonal flows. *Icarus*, *137*(2), 357–359. https://doi.org/10.1006/icar.1998.6064

Iess, L., Folkner, W. M., Durante, D., Parisi, M., Kaspi, Y., Galanti, E., et al. (2018). Measurement of Jupiter's asymmetric gravity field. *Nature*, *555*, 220–222 https://doi.org/10.1038/nature25776

Jacobson, R. A. (2013). JUP310 satellite ephemeris file release. https://naif.jpl.nasa.gov/pub/naif/generic_kernels/spk/satellites/jup310.cmt

Kaspi, Y. (2013). Inferring the depth of the zonal jets on Jupiter and Saturn from odd gravity harmonics. *Geophysical Research Letters*, *40*(4), 676–680. https://doi.org/10.1029/2012GL053873

Kaspi, Y., Flierl, G. R., & Showman, A. P. (2009). The deep wind structure of the giant planets: Results from an anelastic general circulation model. *Icarus*, *202*(2), 525–542. https://doi.org/10.1016/j.icarus.2009.03.026

Kaspi, Y., Galanti, E., Hubbard, W. B., Stevenson, D. J., Bolton, S. J., Iess, L., et al. (2018). Jupiter's atmospheric jet-streams extend thousands of kilometers deep. *Nature*, *555*(7695), 223–226. https://doi.org/10.1038/nature25793

Kaspi, Y., Galanti, E., Showman, A. P., Stevenson, D. J., Gulliot, T., Iess, L. & Bolton, S. J. (2020). Comparison of the deep atmospheric dynamics of Jupiter and Saturn in light of the Juno and Cassini gravity measurements. *Space Science Reviews*. *216*(5), 84. https://doi.org/10.1007/s11214-020-00705-7

Kaspi, Y., Hubbard, W. B., Showman, A. P., & Flierl, G. R. (2010). The gravitational signature of Jupiter's internal dynamics. *Geophysical Research Letters*, *37*(1), L01204. https://doi.org/10.1029/2009GL041385

Parisi, M. (2020). Models of the gravity field of Jupiter using lepian and spherical harmonic functions. *Zenodo*. https://doi.org/10.5281/zenodo.3924390

Parisi, M., Folkner, W. M., Galanti, E., Kaspi, Y., Buccino, D. R., Oudrhiri, K., et al. (2020). A mascon approach to estimating the depth of Jupiter's Great Red Spot with Juno gravity measurements. *Planetary and Space Science*, *181*, 104781. https://doi.org/10.1016/j.pss.2019.104781

Parisi, M., Galanti, E., Finocchiaro, S., Iess, L., & Kaspi, Y. (2016). Probing the depth of Jupiter's Great Red Spot with the Juno gravity experiment. *Icarus*, *267*, 232–242. https://doi.org/10.1016/j.icarus.2015.12.011

Phipps, P. H., Withers, P., Buccino, D. R., Yang, Y.-M., & Parisi, M. (2019). Variations in the density distribution of the Io plasma torus as seen by radio occultations on Juno Perijoves 3, 6, and 8. *Journal of Geophysical Research Space Physics*, *124*(7), 5200–5221. https://doi.org/10.1029/2018JA026297

Plattner, A., & Simons, F. J. (2017). Internal and external potential-field estimation from regional vector data at varying satellite altitude. *Geophysical Journal International*, *211*(1), 207–238. https://doi.org/10.1093/gji/ggx244

Simons, F. J., & Dahlen, F. A. (2006). Spherical Slepian functions and the polar gap in geodesy. *Geophysical Journal International*, *166*(3), 1039–1061. https://doi.org/10.1111/j.1365-246X.2006.03065.x

Simons, F. J., Dahlen, F. A., & Wieczorek, M. A. (2006). Spatiospectral concentration on a sphere. *SIAM Review*, *48*(3), 504–536. https://doi.org/10.1137/S0036144504445765

Simons, F. J., Hawthorne, J. C., & Beggan, C. D. (2009). Efficient analysis and representation of geophysical processes using localized spherical basis functions. Proceedings of SPIE, 7446, Wavelets XIII, 74460G. https://doi.org/10.1117/12.825730

Tollefson, J., Wong, M. H., de Pater, I., Simon, A. A., Orton, G. S., Rogers, J. H., et al. (2017). Changes in Jupiter's zonal wind profile preceding and during the Juno mission. *Icarus*, *296*, 163–178. https://doi.org/10.1016/j.icarus.2017.06.007

Wahl, S. M., Parisi, M., Folkner, W. M., Hubbard, W. B., & Militzer, B. (2020). Equilibrium tidal response of jupiter: Detectability by the Juno spacecraft. *The Astrophysical Journal*, *891*(1). https://doi.org/10.3847/1538-4357/ab6cf9

Wieczorek, M. A., & Simons, F. J. (2005). Localized spectral analysis on the sphere. *Geophysical Journal International*, *162*(3), 655–675. https://doi.org/10.1111/j.1365-246X.2005.02687.x